Interference effects on the transport characteristics of a benzene single-electron transistor

D. Darau, G. Begemann, A. Donarini, and M. Grifoni
Institut für Theoretische Physik, Universität Regensburg, 93035 Regensburg, Germany
(Received 14 October 2008; revised manuscript received 18 February 2009; published 9 June 2009)

Interference effects strongly affect the transport characteristics of a benzene single-electron transistor, and for this reason we call it interference single-electron transistor (I-SET). We focus on the effects of degeneracies between many-body states of the isolated benzene. We show that the particular current blocking and selective conductance suppression occurring in the benzene I-SET are due to *interference* effects between the orbitally degenerate states. Further we study the impact of reduced symmetry due to anchor groups or potential drop over the molecule. We identify in the *quasidegeneracy* of the involved molecular states the necessary condition for the robustness of the results.

DOI: 10.1103/PhysRevB.79.235404 PACS number(s): 85.65.+h, 85.85.+j

I. INTRODUCTION

Molecular electronics, due to perfect reproducibility and versatile chemical tailoring of its basic components, represents one of the most promising answers to the increasing miniaturization demand of information technology. A crucial issue in molecular electronics is thus the understanding of the conduction characteristics through single molecules.[1]

Single-molecule-transport measurements rely on the fabrication of a nanogap between source and drain electrodes and the formation of a stable molecule-electrode contact. Nanogaps are nowadays routinely obtained using different techniques including electromigration,[2–10] mechanical break-junction,[11–14] and scanning tunneling microscopy.[15–17] Also the challenging goal of effectively gating a nanometer-sized molecule in the presence of macroscopic metallic leads has been achieved.[6,14,18]

A stable contact between molecule and leads is commonly realized with the mediation of anchor groups attached to the molecule during its chemical synthesis. Also direct coupling of the molecule to the electric leads, though, has been very recently reported.[13] One of the advantages of the first connecting method is some control over the contact configuration of the molecule[19] and the possibility of designing the strength of the tunneling coupling by choosing specific anchor groups.[6,17,20,21] All previous achievements combined with the experience accumulated with semiconducting and carbon-based single-electron transistors (SETs) allowed in recent years to measure stability diagrams of single-molecule transistor devices thus realizing molecular spectroscopy via transport experiments.[2–10]

Single-molecule transistors display transport properties which are very different from those of conventional single-electron transistors. In fact, vibrational or torsional modes[7,10] and intrinsic symmetries of the molecule can hinder or favor transport through the molecular SET, visible, e.g., in the absence or presence of specific excitation lines in the stability diagram or in negative differential conductance features. Many-body phenomena as, e.g., the Kondo effect, have been observed as well.[2,3,5,10,22]

Despite the experimental progress, the theoretical understanding of the properties of single organic molecules coupled to electrodes is far from being satisfactory. On one hand, numerical approaches to transport based on the combination of Green's-function methods with tight-binding model or density functional theory have become standard in the study of transport at the nanoscale.[1] These methods are appropriate to investigate quantum transport through molecular bridges strongly coupled to leads. In this regime various groups have recently discussed the possibility of observing interference effects,[23–26] e.g., in conjugated monocyclic molecules as benzene or annulene.[23,25] However, for the description of transport through a molecule weakly coupled to leads, other methods are required. In the Coulomb blockade regime, for example, due to the crucial role played by the Coulomb interaction in these systems it is common to resort to a Pauli rate equation[27] or to a generalized master equation for the reduced density matrix (RDM). For example, in the work of Hettler *et al.*,[28] an electronic structure calculation has been performed in order to construct an effective interacting Hamiltonian for the π orbitals of benzene, and the I-V characteristics of the corresponding molecular junction have been calculated within the rate equation approach.

In the presence of degenerate states, however, coherences of the density matrix influence the dynamics and a master equation approach is appropriate.[29–38] Such coherences can give rise to precession effects in spin transport[30,35] or cause interference in a molecular single-electron transistor.[32,35,37] In the present work we wish to generalize the discussion on interference phenomena in a benzene interference SET presented in Ref. 37 to the case in which the perfect degeneracy is broken due, e.g., to contact effects or to the applied external bias. To this extent the master equation used in Ref. 37 will be generalized to treat the case of quasidegenerate states. Conditions for the persistence of interference phenomena are identified. We observe that the effects of quasidegenerate states on transport have been very recently addressed also in Ref. 38. We treat the transport through the benzene I-SET in two different setups, the para and the metaconfiguration, depending on the position of the leads with respect to the benzene molecule (see Fig. 1). Similar to Ref. 28, we start from an interacting Hamiltonian of isolated benzene where only the localized p_z orbitals are considered and the ions are assumed to have the same spatial symmetry as the relevant electrons. We calculate the $4^6=4096$ energy eigenstates of the benzene Hamiltonian numerically.

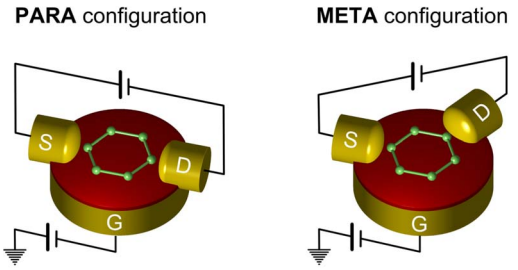

FIG. 1. (Color online) Schematic representation of the two different setups for the benzene I-SET considered in this paper. The molecule, lying on a dielectric substrate, is weakly contacted to source and drain leads as well as capacitively gated.

Subsequently, with the help of group theory, we classify the eigenstates according to their different symmetries and thus give a group-theoretical explanation to the large degeneracies occurring between the electronic states. For example, while the six-particle ground state (A_{1g} symmetry) is nondegenerate, there exist four seven-particle ground states due to spin and orbital (E_{2u} symmetry) degeneracies. Fingerprints of these orbital symmetries are clearly visible in the strong differences in the stability diagrams obtained by coupling the benzene I-SET to the leads in the meta and paraconfiguration. Striking are the selective reduction conductance and the appearance of regions of interference-driven current blocking with associated negative differential conductance (NDC) when changing from the para to the metaconfiguration.

NDC and current blocking for benzene junctions have been predicted in Ref. 28 but also in the paraconfiguration *and* in the presence of an external electromagnetic field. In our work NDC occurs despite the absence of an external field in the unperturbed setup and with no asymmetry in the tunneling rates. In fact, NDC and current blocking triggered by interference take place any time a SET presents an N-particle nondegenerate state and two degenerate $N+1$-particle states such that the ratio between the transition *amplitudes* $\gamma_{i\alpha}$ ($i=1,2$, $\alpha=L,R$) between those N- and $N+1$-particle states is different for tunneling at the left (L) and at the right (R) lead,

$$\frac{\gamma_{1\mathrm{L}}}{\gamma_{2\mathrm{L}}} \neq \frac{\gamma_{1\mathrm{R}}}{\gamma_{2\mathrm{R}}}. \tag{1}$$

Notice that no asymmetry in the tunneling *rates*, which are proportional to $|\gamma_{i\alpha}|^2$, is implied by Eq. (1). This fact excludes the interpretation of the physics of the interference-SET in terms of standard NDC with asymmetric couplings. Due to condition (1) there exist linear combinations of the degenerate $N+1$-particle states which are coupled to one of the leads but *not* to the other. The state that is decoupled from the right lead represents a blocking state for the current flowing $L\rightarrow R$ since electrons can populate this state by tunneling from the left lead but cannot tunnel out toward the right lead. Vice versa the state decoupled from the left lead is a blocking state for the current $R\rightarrow L$. Typically these two blocking states are not orthogonal and thus cannot form together a valid basis set. The basis set that diagonalizes the stationary density matrix (what we call in the manuscript as the "physical basis") contains at large positive biases the $L\rightarrow R$ blocking state and is thus different from the physical basis at large negative biases which necessarily contains the $R\rightarrow L$ blocking state. More generally the "physical basis" *depends continuously* on the bias. Thus only a treatment that includes coherences in the density matrix can capture the full picture at all biases. By neglecting for simplicity the spin degree of freedom, the seven-particle ground state of benzene is two times degenerate while the six-particle one is nondegenerate. If we choose for the seven-particle states the eigenstates of the z projection of the angular momentum we obtain the relation

$$\frac{\gamma_{1\mathrm{L}}}{\gamma_{2\mathrm{L}}} = \frac{\gamma_{1\mathrm{R}}}{\gamma_{2\mathrm{R}}} e^{4i\phi}, \tag{2}$$

where ϕ is the angle between the left and the right leads. Thus in the metaconfiguration ($\phi=2\pi/3$) condition (1) is fulfilled, while in the paraconfiguration ($\phi=\pi$) the amplitude ratios are equal. This condition implies that in the paraconfiguration one of the seven-particle states is decoupled from *both* leads at the same time and can thus (in first approximation) be excluded from the dynamics. In contrast, in the metaconfiguration, the linear combination of uniformly distributed eigenstates of the angular momentum creates states with a peculiar interference pattern. The position of their nodes allows to characterize them as different blocking states.

This paper is outlined as follows: in Sec. II we introduce the model Hamiltonian of the system and present a density matrix approach setting up a generalized master equation describing the electron dynamics. We give the expression for the current in the fully symmetric setup [the generalized master equation (GME) and the current formula for the setup under perturbation are given in Appendix A]. Further we provide a detailed analysis of the symmetry characteristics of the molecular eigenstates.

In Sec. III we present numerical and analytical results of transport calculations for the unperturbed setup. We study the occurring interference effects and provide an explanation of the phenomena based on symmetry considerations.

In Sec. IV we present the results for the perturbed setup including a detailed discussion of the transport in this case. We identify in the *quasidegeneracy* of the contributing molecular states the necessary condition for the robustness of the interference effects. Conclusions and remarks are presented in Sec. V.

II. MODEL HAMILTONIAN AND DENSITY MATRIX APPROACH

A. Model Hamiltonian

For the description of the benzene molecule weakly coupled to source and drain leads, we adopt the total Hamiltonian $H=H^0_{\mathrm{ben}}+H_{\mathrm{leads}}+H_{\mathrm{T}}+H'_{\mathrm{ben}}$. The first term is the interacting Hamiltonian for isolated benzene,[39–41]

$$H_{\text{ben}}^0 = \xi_0 \sum_{i\sigma} d_{i\sigma}^\dagger d_{i\sigma} + b \sum_{i\sigma} (d_{i\sigma}^\dagger d_{i+1\sigma} + d_{i+1\sigma}^\dagger d_{i\sigma}) + U \sum_i \left(n_{i\uparrow} - \tfrac{1}{2}\right)\left(n_{i\downarrow} - \tfrac{1}{2}\right) + V \sum_i (n_{i\uparrow} + n_{i\downarrow} - 1)(n_{i+1\uparrow} + n_{i+1\downarrow} - 1), \quad (3)$$

where $d_{i\sigma}^\dagger$ creates an electron of spin σ in the p_z orbital of carbon i; $i=1,\ldots,6$ runs over the six carbon atoms of benzene and $n_{i\sigma}=d_{i\sigma}^\dagger d_{i\sigma}$.

Only the p_z orbitals (one per carbon atom) are explicitly taken into account, while the core electrons and the nuclei are combined into frozen ions, with the same spatial symmetry as the relevant electrons. They contribute only to the constant terms of the Hamiltonian and enforce particle-hole symmetry. Mechanical oscillations are neglected, and all atoms are considered at their equilibrium position.

This Hamiltonian for isolated benzene is respecting the D_{6h} symmetry of the molecule. Since for every site there are four different possible configurations $(|0\rangle, |\uparrow\rangle, |\downarrow\rangle, |\uparrow\downarrow\rangle)$, the Fock space has the dimension $4^6=4096$, which requires a numerical treatment. Although the diagonalization of the Hamiltonian is not a numerical challenge, it turns out to be of benefit for the physical understanding of the transport processes to divide H_{ben} into blocks, according to the number N of p_z electrons (from 0 to 12), the z projection S_z of the total spin, and the orbital symmetries of benzene (see Table I).

The parameters b, U, and V for isolated benzene are given in the literature[42] and are chosen to fit optical excitation spectra. The presence of metallic electrodes and the dielectric in the molecular I-SET, is expected to cause a substantial renormalization of U and V.[4,43] Nevertheless, we do not expect the main results of this work to be affected by this change. We consider the benzene molecule weakly coupled to the leads. Thus, to first approximation, we assume the symmetry of the isolated molecule not to be changed by the screening. Perturbations due to the lead-molecule contacts reduce the symmetry in the molecular junction. They are included in H'_{ben} [see Eqs. (24) and (25)] and will be treated in Sec. IV.

The effect of the gate is included as a renormalization of the on-site energy $\xi=\xi_0-eV_g$ (V_g is the gate voltage), and we conventionally set $V_g=0$ at the charge neutrality point. Source and drain leads are two reservoirs of noninteracting electrons: $H_{\text{leads}}=\Sigma_{\alpha k\sigma}(\epsilon_k-\mu_\alpha)c_{\alpha k\sigma}^\dagger c_{\alpha k\sigma}$, where $\alpha=L,R$ stands for the left or right lead and the chemical potentials μ_α of the leads depend on the applied bias voltage $\mu_{L,R}=\mu_0 \pm \frac{V_b}{2}$. In the following we will measure the energy starting from the equilibrium chemical potential $\mu_0=0$. The coupling to source and drain leads is described by the tunneling Hamiltonian

$$H_T = t \sum_{\alpha k\sigma} (d_{\alpha\sigma}^\dagger c_{\alpha k\sigma} + c_{\alpha k\sigma}^\dagger d_{\alpha\sigma}), \quad (4)$$

where we define $d_{\alpha\sigma}^\dagger$ as the creator of an electron in the benzene carbon atom which is closest to the lead α. In particular $d_{R\sigma}^\dagger := d_{4\sigma}^\dagger, d_{5\sigma}^\dagger$, respectively, in the para and metaconfiguration, while $d_{L\sigma}^\dagger := d_{1\sigma}^\dagger$ in both setups.

TABLE I. Overview of the six-particle states of benzene, sorted by S_z and symmetry. Orbitals with A- and B-types of symmetry show no degeneracy, while E-type orbitals are doubly degenerate.

N	No. of ↑	No. of ↓	No. of states	No. of states with a certain symmetry
6	6	0	1	$1\ B_{1u}$
	5	1	36	$4\ A_{1g}$ $2\ A_{2g}$ $2\times 6\ E_{2g}$ $4\ B_{1u}$ $2\ B_{2u}$ $2\times 6\ E_{1u}$
	4	2	225	$16\ A_{1g}$ $20\ A_{2g}$ $2\times 36\ E_{2g}$ $22\ B_{1u}$ $17\ B_{2u}$ $2\times 39\ E_{1u}$
	3	3	400	$38\ A_{1g}$ $30\ A_{2g}$ $2\times 66\ E_{2g}$ $38\ B_{1u}$ $30\ B_{2u}$ $2\times 66\ E_{1u}$
	2	4	225	⋮
	1	5	36	
	0	6	1	

B. Dynamics of the reduced density matrix

Given the high degeneracy of the spectrum, the method of choice to treat the dynamics in the weak coupling is the Liouville equation method already used, e.g., in Refs. 32 and 34. In this section we shortly outline how to derive the equation of motion for the RDM to lowest nonvanishing order in the tunneling Hamiltonian. For more details we refer to Refs. 34 and 35.

Starting point is the Liouville equation for the total density operator of molecule and leads ρ in the interaction picture, treating H_T as a perturbation: $i\hbar\frac{d\rho^I(t)}{dt}=[H_T^I,\rho^I(t)]$. This equation integrated over time and iterated to the second order reads as

$$\dot{\rho}^I(t) = -\frac{i}{\hbar}[H_T^I(t),\rho^I(t_0)] - \frac{1}{\hbar^2}\int_{t_0}^t dt'[H_T^I(t),[H_T^I(t'),\rho^I(t')]]. \quad (5)$$

Since we are only interested in the transport through the molecule, we treat from now on the time evolution of the RDM $\sigma=\text{Tr}_{\text{leads}}\{\rho^I(t)\}$,[44] which is formally obtained from Eq. (5) by tracing out the lead degrees of freedom: $\dot{\sigma}=\text{Tr}_{\text{leads}}\{\dot{\rho}^I\}$.

In order to proceed, we make the following standard approximations:

(i) the leads are considered as reservoirs of noninteracting electrons in thermal equilibrium. Hence we can factorize the density matrix as $\rho^{\mathrm{I}}(t)=\sigma(t)\rho_{\mathrm{s}}\rho_{\mathrm{d}}=\sigma(t)\rho_{\mathrm{leads}}$.

(ii) Since the molecule is weakly coupled to the leads we treat the effects of H_{T} to the lowest nonvanishing order.

(iii) Due to the continuous interaction of the system with the leads and at high enough temperature, it is legitimate to apply the Markov approximation and obtain an equation for $\dot{\sigma}$ which is local in time [$\sigma(t)$ instead of $\sigma(t')$ inside the integral]. In particular the Markov approximation becomes exact in the stationary limit ($t\to\infty$) we will focus on. Since we are interested in the long-term behavior of the system, we set $t_0\to-\infty$ in Eq. (5) and finally obtain the GME,

$$\dot{\sigma}(t)=\frac{-1}{\hbar^2}\int_0^\infty dt''\ \mathrm{Tr}_{\mathrm{leads}}\{[H_{\mathrm{T}}^{\mathrm{I}}(t),[H_{\mathrm{T}}^{\mathrm{I}}(t-t''),\sigma(t)\rho_{\mathrm{leads}}]]\}. \tag{6}$$

The reduced density operator σ is defined on the Fock space of benzene, yet we can neglect coherences between states with different particle number since they are decoupled from the dynamics of the populations. For simplicity, we continue here the derivation of the GME only for the symmetric case with exact orbital degeneracy, i.e., neglecting H'_{ben} (the perturbed case is presented in Appendix A).

(iv) Further we also neglect coherences between states with different energy (secular approximation). They are irrelevant due to their fast fluctuation compared to the dynamics of the system triggered by the tunneling coupling.

Under these considerations, it is convenient to express the GME in terms of the reduced density operator $\sigma^{\mathrm{NE}}=\mathcal{P}_{\mathrm{NE}}\sigma\mathcal{P}_{\mathrm{NE}}$, where $\mathcal{P}_{\mathrm{NE}}:=\Sigma_{\ell\tau}|NE\ell\tau\rangle\langle NE\ell\tau|$ is the projection operator on the subspace of N particles and energy E. The sum runs over the orbital and spin quantum numbers ℓ and τ, respectively. The orbital quantum number ℓ distinguishes between orbitally degenerate states. The exact meaning of ℓ will be illustrated in the next section. In Appendix A we derive a GME that retains coherences also between quasidegenerate states. That approach treats with special care the small asymmetries introduced in the molecule by the coupling to the leads. In fact it interpolates between the degenerate case treated here and the fully nondegenerate case in which the GME reduces to a master equation for populations only. Equation (6) can be further manipulated by projection into the subspace of N particle and energy E. Since we assume the density matrix to be factorized and the leads to be in thermal equilibrium, also the traces over the leads degree of freedom can be easily performed. Eventually, the GME for the degenerate case reads as

$$\begin{aligned}\dot{\sigma}^{\mathrm{NE}}=&-\sum_{\alpha\tau}\frac{\Gamma_\alpha}{2}\Bigg\{\mathcal{P}_{\mathrm{NE}}d_{\alpha\tau}\left[f_\alpha^+(H_{\mathrm{ben}}^0-E)-\frac{i}{\pi}p_\alpha(H_{\mathrm{ben}}^0-E)\right]d_{\alpha\tau}^\dagger\sigma^{\mathrm{NE}}\\&+\mathcal{P}_{\mathrm{NE}}d_{\alpha\tau}^\dagger\left[f_\alpha^-(E-H_{\mathrm{ben}}^0)-\frac{i}{\pi}p_\alpha(E-H_{\mathrm{ben}}^0)\right]d_{\alpha\tau}\sigma^{\mathrm{NE}}+\mathrm{H.c.}\Bigg\}\\&+\sum_{\alpha\tau\mathrm{E}'}\Gamma_\alpha\mathcal{P}_{\mathrm{NE}}\{d_{\alpha\tau}^\dagger f_\alpha^+(E-E')\sigma^{\mathrm{N-1E}'}d_{\alpha\tau}+d_{\alpha\tau}f_\alpha^-(E'-E)\sigma^{\mathrm{N+1E}'}d_{\alpha\tau}^\dagger\}\mathcal{P}_{\mathrm{NE}},\end{aligned} \tag{7}$$

where $\Gamma_{\mathrm{L,R}}=\frac{2\pi}{\hbar}|t_{\mathrm{L,R}}|^2\mathcal{D}_{\mathrm{L,R}}$ are the bare transfer rates with the constant densities of states of the leads $\mathcal{D}_{\mathrm{L,R}}$. Terms describing sequential tunneling from and to the lead α are proportional to the Fermi functions $f_\alpha^+(x):=f(x-\mu_\alpha)$ and $f_\alpha^-(x):=1-f_\alpha^+(x)$, respectively. Still in the sequential tunneling limit, but only in the equations for the coherences, one finds also the energy nonconserving terms, proportional to the function $p_\alpha(x)=-\mathrm{Re}\ \psi[\frac{1}{2}+\frac{i\beta}{2\pi}(x-\mu_\alpha)]$, where ψ is the digamma function. Both the Fermi functions and the digamma function result from the trace over the lead degrees of freedom.[30,34,44]

A closer analysis of the master equation allows also the formulation of an expression for the current operator. We start from the definition of the time derivative of the charge on benzene,

$$\frac{d}{dt}\langle Q\rangle=\mathrm{Tr}\{\hat{N}\dot{\sigma}\}=\langle I_{\mathrm{L}}+I_{\mathrm{R}}\rangle, \tag{8}$$

where $Q=\Sigma_{i\tau}(d_{i\tau}^\dagger d_{i\tau}-6)$ is the operator of the charge on benzene, $\hat{N}$ is the particle number operator, and $I_{\mathrm{L,R}}$ are the current operators at the left (right) contact. Conventionally, in the definition of $I_{\mathrm{L,R}}$ we assume the current to be positive when it is increasing the charge on the molecule. Thus, in the stationary limit, $\langle I_{\mathrm{L}}+I_{\mathrm{R}}\rangle$ is zero. We write this expression in the basis of the subspaces of N particles and energy E,

$$\langle I_{\mathrm{L}}+I_{\mathrm{R}}\rangle=\sum_{\mathrm{NE}}\mathrm{Tr}\{\hat{N}\mathcal{P}_{\mathrm{NE}}\dot{\sigma}\mathcal{P}_{\mathrm{NE}}\}=\sum_{\mathrm{NE}}\mathrm{Tr}\{N\dot{\sigma}^{\mathrm{NE}}\}. \tag{9}$$

Further we insert Eq. (7) in Eq. (9) and take advantage of the cyclic properties of the trace to find

$$\langle I_L + I_R \rangle = \sum_{NE} \sum_{\alpha\tau} N\Gamma_\alpha \, \mathrm{Tr}\Big\{ -[f_\alpha^+(H_{ben}^0 - E) d_{\alpha\tau}^\dagger \sigma^{NE} d_{\alpha\tau} + f_\alpha^-(E - H_{ben}^0) d_{\alpha\tau} \sigma^{NE} d_{\alpha\tau}^\dagger] + \sum_{E'} \mathcal{P}_{NE}[f_\alpha^+(E - E') \times d_{\alpha\tau}^\dagger \sigma^{N-1E'} d_{\alpha\tau} + f_\alpha^-(E' - E) d_{\alpha\tau} \sigma^{N+1E'} d_{\alpha\tau}^\dagger] \Big\}. \tag{10}$$

Notice that the energy nonconserving contributions drop from the expression of the current. Still they contribute to the average current via the density matrix. Since E and E' are dummy variables, we can switch them in the summands containing E'. Applying the relation

$$\sum_{NE'} \mathrm{Tr}\{\mathcal{P}_{NE'} g(E')\} = \mathrm{Tr}\{g(H_{ben}^0)\},$$

where $g(E')$ is a generic function, we substitute E' with H_{ben}^0 in Eq. (10). Further we can conveniently rearrange the sum over N, arriving at the expression for the current,

$$\langle I_L + I_R \rangle = \sum_{NE} \sum_{\alpha\tau} \Gamma_\alpha \, \mathrm{Tr} \{ d_{\alpha\tau}^\dagger \sigma^{NE} d_{\alpha\tau} [-N f_\alpha^+(H_{ben}^0 - E) + (N+1) f_\alpha^+(H_{ben}^0 - E)] + d_{\alpha\tau} \sigma^{NE} d_{\alpha\tau}^\dagger [-N f_\alpha^-(E - H_{ben}^0) + (N-1) f_\alpha^-(E - H_{ben}^0)] \}. \tag{11}$$

This relation can be further simplified in order to identify the current operators. The one corresponding to the left contact is, e.g.,

$$I_L = \Gamma_L \sum_{NE\tau} \mathcal{P}_{NE}[d_{L\tau} f_L^+(H_{ben}^0 - E) d_{L\tau}^\dagger + - d_{L\tau}^\dagger f_L^-(E - H_{ben}^0) d_{L\tau}] \mathcal{P}_{NE}. \tag{12}$$

With this relation we can calculate the stationary current as the average $\langle I_L \rangle = \mathrm{Tr}\{\sigma_{stat} I_L\} = -\langle I_R \rangle$, with σ_{stat} as the stationary density operator. The expression of the current operator for the perturbed system is given in Appendix A.

C. Symmetry of the benzene eigenstates

In this section, we will review the symmetry characteristics of the eigenstates of the interacting Hamiltonian of benzene, focusing on the symmetry operations σ_v and C_n which have a major impact on the electronic transport through the molecular I-SET. Benzene belongs to the D_{6h} point group. Depending on their behavior under symmetry operations, one can classify the molecular orbitals by their belonging to a certain irreducible representation of the point group.

Table I shows an overview of the states of the neutral molecule (the six-particle states) sorted by S_z and symmetries. The eigenstates of the interacting benzene molecule have either A-, B-, or E-type symmetries. While orbitals having A or B symmetries can only be spin degenerate, states with an E symmetry show an additional twofold orbital degeneracy, essential for the explanation of the transport features occurring in the metaconfiguration.

TABLE II. Degeneracy, energy, and symmetry of the ground states of the isolated benzene molecule for different particle numbers. We choose the on-site and intersite Coulomb interactions to be $U=10$ eV and $V=6$ eV, and the hopping to be $b=-2.5$ eV. Notice, however, that screening effects from the leads and the dielectric are expected to renormalize the energy of the benzene many-body states.

N	Degeneracy	Energy(at $\xi=0$) [eV]	Symmetry	Symmetry behavior under σ_v
0	1	0	A_{1g}	sym
1	2	−22	A_{2u}	sym
2	1	−42.25	A_{1g}	sym
3	4	−57.42	E_{1g}	2 sym, [2 antisym]
4	[3]	[−68.87]	$[A_{2g}]$	[antisym]
	2	−68.37	E_{2g}	1 sym, [1 antisym]
5	4	−76.675	E_{1g}	2 sym, [2 antisym]
6	1	−81.725	A_{1g}	sym
7	4	−76.675	E_{2u}	2 sym, [2 antisym]
8	[3]	[−68.87]	$[A_{2g}]$	[antisym]
	2	−68.37	E_{2g}	1 sym, [1 antisym]
9	4	−57.42	E_{2u}	2 sym, [2 antisym]
10	1	−42.25	A_{1g}	sym
11	2	−22	B_{2g}	sym
12	1	0	A_{1g}	sym

Transport at low bias is described in terms of transitions between ground states with different particle number. Table II shows the symmetries of the ground states (and of some first excited states) of interacting benzene for all possible particle numbers. Ground-state transitions occur both between orbitally nondegenerate states (with A and B symmetries), as well as between orbitally degenerate and nondegenerate states (E- to A-type states).

The interacting benzene Hamiltonian commutes with all the symmetry operations of the D_{6h} point group; thus, it has a set of common eigenvectors with each operation. The element of D_{6h} of special interest for the *para*configuration is σ_v, i.e., the reflection about the plane through the contact atoms and perpendicular to the molecular plane. The molecular orbitals with A and B symmetries are eigenstates of σ_v with eigenvalue of ± 1; i.e., they are either symmetric or antisymmetric with respect to the σ_v operation. The behavior of the E-type orbitals under σ_v is basis dependent, yet one can always choose a basis in which one orbital is symmetric and the other one antisymmetric.

Let us now consider the generic transition amplitude $\langle N | d_{\alpha\tau} | N+1 \rangle$, where $d_{\alpha\tau}$ destroys an electron of spin τ on the contact atom closest to the α lead. It is useful to rewrite this amplitude in the form

$$\langle N | d_{\alpha\tau} | N+1 \rangle = \langle N | \sigma_v^\dagger \sigma_v d_{\alpha\tau} \sigma_v^\dagger \sigma_v | N+1 \rangle, \tag{13}$$

where we have used the property $\sigma_v^\dagger \sigma_v = 1$. Since in the para-configuration both contact atoms lie in the mirror plane σ_v, it

follows that $\sigma_v d_\alpha \sigma_v^\dagger = d_\alpha$. If the participating states are both symmetric or both antisymmetric under σ_v, Eq. (13) is trivial. For states with different symmetry it is

$$\langle N, \mathrm{sym}|d_{\alpha\tau}|N+1, \mathrm{antisym}\rangle = -\langle N, \mathrm{sym}|d_{\alpha\tau}|N+1, \mathrm{antisym}\rangle, \tag{14}$$

implying that the matrix element vanishes. In other terms, there is a selection rule that forbids transitions between symmetric and antisymmetric states. Further, since the ground state of the neutral molecule is symmetric, for the transport calculations in the paraconfiguration we select the effective Hilbert space containing only states symmetric with respect to σ_v. Correspondingly, when referring to the N-particle ground state we mean the energetically lowest *symmetric* state. For example, in the case of four- and eight-particle states it is the first excited state to be the *effective* ground state. In the paraconfiguration also the orbital degeneracy of the E-type states is effectively cancelled due to the selection of the symmetric orbital (see Table II).

Small violations of this selection rule, due, e.g., to molecular vibrations or coupling to an electromagnetic bath, result in the weak connection of different metastable electronic subspaces. We suggest this mechanism as a possible explanation for the switching and hysteretic behavior reported in various molecular junctions. This effect is not addressed in this work.

For a simpler analysis of the different transport characteristics it is useful to introduce a unified geometrical description of the two configurations. In both cases, one lead is rotated by an angle ϕ with respect to the position of the other lead. Hence we can write the creator of an electron in the right contact atom $d_{R\tau}^\dagger$ in terms of the creation operator of the left contact atom and the rotation operator,

$$d_{R\tau}^\dagger = \mathcal{R}_\phi^\dagger d_{L\tau}^\dagger \mathcal{R}_\phi, \tag{15}$$

where $\mathcal{R}_\phi$ is the rotation operator for the anticlockwise rotation of an angle ϕ around the axis perpendicular to the molecular plane and piercing the center of the benzene ring; $\phi = \pi$ for the paraconfiguration and $\phi = (2\pi/3)$ for the metaconfiguration.

The energy eigenstates of the interacting Hamiltonian of benzene can be classified also in terms of their quasiangular momentum. In particular, the eigenstates of the z projection of the quasiangular momentum are the ones that diagonalize all operators $\mathcal{R}_\phi$ with angle multiples of $\pi/3$. The corresponding eigenvalues are phase factors $e^{-i\ell\phi}$ where $\hbar\ell$, the quasiangular momentum of the state, is an integer multiple of $\hbar$. The discrete rotation operator of an angle $\phi = \pi$ (C_2 symmetry operation) is the one relevant for the paraconfiguration. All orbitals are eigenstates of the C_2 rotation with the eigenvalue of ± 1.

The relevant rotation operator for the metaconfiguration corresponds to an angle $\phi = 2\pi/3$ (C_3 symmetry operation). Orbitals with an A or B symmetry are eigenstates of this operator with the eigenvalue of +1 (angular momentum $\ell = 0$ or $\ell = 3$). Hence we can already predict that there will be no difference based on rotational symmetry between the paraconfiguration and the metaconfiguration for transitions between states involving A- and B-type symmetries. Orbitals with E symmetry however behave quite differently under the C_3 operation. They are the pairs of states of angular momenta $\ell = \pm 1$ or $\ell = \pm 2$. The diagonal form of the rotation operator on the twofold degenerate subspace of E symmetry reads as

$$C_3 = \begin{pmatrix} e^{-i|\ell|2\pi/3} & 0 \\ 0 & e^{i|\ell|2\pi/3} \end{pmatrix}. \tag{16}$$

For the twofold orbitally degenerate seven-particle ground states $|\ell| = 2$. This analysis in terms of the quasiangular momentum makes the calculation of the fundamental interference condition [Eq. (2)] given in Sec. I easier. In fact the following relation holds between the transition amplitudes of the six- and seven-particle ground states:

$$\gamma_{\ell R} \equiv \langle 7_g \ell\tau|d_{R\tau}^\dagger|6_g\rangle = \langle 7_g \ell\tau|\mathcal{R}_\phi^\dagger d_{L\tau}^\dagger \mathcal{R}_\phi|6_g\rangle = e^{-i\ell\phi}\gamma_{\ell L}, \tag{17}$$

and Eq. (2) follows directly.

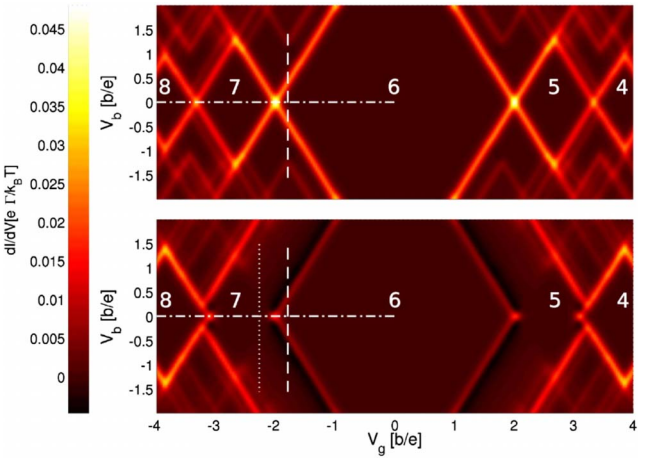

FIG. 2. (Color online) Stability diagram for the benzene I-SET contacted in the para (above) and metaconfiguration (below). Dot-dashed lines highlight the conductance cuts presented in Fig. 3, the dashed lines mark the regions corresponding to the current traces presented in Figs. 4 and 6, and the dotted line is the region corresponding to the current trace presented in Fig. 5. The parameters used are $U = 4|b|$, $V = 2.4|b|$, $k_B T = 0.04|b|$, $\hbar\Gamma_L = \hbar\Gamma_R = 10^{-3}|b|$.

III. TRANSPORT CALCULATIONS: FULLY SYMMETRIC SETUP

With the knowledge of the eigenstates and eigenvalues of the Hamiltonian for the isolated molecule, we implement Eq. (7) and look for a stationary solution. The symmetries of the eigenstates are reflected in the transition amplitudes contained in the GME. We find numerically its stationary solution and calculate the current and the differential conductance of the device. In Fig. 2 we present the stability diagram for the benzene I-SET contacted in the paraconfiguration (upper panel) and metaconfiguration (lower panel). Bright ground-state transition lines delimit diamonds of zero differential conductance typical for the Coulomb blockade regime,

while a rich pattern of satellite lines represents the transitions between excited states. Though several differences can be noticed, most striking are the suppression of the linear conductance, the appearance of negative differential conductance (NDC), and the strong suppression of the current at the right (left) border of the seven- (five-) particle diamond when passing from the para to the metaconfiguration. All these features are different manifestations of the interference between orbitally degenerate states and ultimately reveal the specific symmetry of benzene.

A. Linear conductance

We study the linear transport regime both numerically and analytically. For the analytical calculation of the conductance we consider the low-temperature limit where only ground states with N and $N+1$ particles have considerable occupation probabilities, with N fixed by the gate voltage. Therefore only transitions between these states are relevant and we can treat just the terms of Eq. (7) with N and $N+1$ particles and the ground-state energies $E_{\mathrm{g,N}}$ and $E_{\mathrm{g,N+1}}$, respectively. A closer look at Eq. (7) reveals that the spin coherences are decoupled from the other elements of the density matrix. Thus we can set them to zero, and write Eq. (7) in a block diagonal form on the basis of the ground states of N and $N+1$ particles. Additionally, since the total Hamiltonian H is symmetric in spin, the blocks of the GME with the same particle but different spin quantum number τ must be identical. Finally, since around the resonance the only populated states are the N- and $N+1$-particle states, the conservation of probability implies that

$$1 = \sum_n \sigma_{nn}^{\mathrm{N}} + \sum_m \sigma_{mm}^{\mathrm{N+1}}, \tag{18}$$

where σ_{nn}^{N} is the population of the N-particle ground state and n contains the orbital and spin quantum numbers. With all these observations we can reduce Eq. (7) to a much smaller set of coupled differential equations, which can be treated analytically. The stationary solution of this set of equations can be derived more easily by neglecting the energy nonconserving terms in Eq. (7). These are contained in the elements of the GME describing the dynamics of the coherences between orbitally degenerate states. With this simplification we derive an analytical formula for the conductance close to the resonance between N- and $N+1$-particle states as the first order coefficient of the Taylor series of the current in the bias,

$$G_{\mathrm{N,N+1}}(\Delta E) = 2e^2 \frac{\Gamma_{\mathrm{L}}\Gamma_{\mathrm{R}}}{\Gamma_{\mathrm{L}}+\Gamma_{\mathrm{R}}} \Lambda_{\mathrm{N,N+1}} \times \left[-\frac{S_{\mathrm{N}} S_{\mathrm{N+1}} f'(\Delta E)}{(S_{\mathrm{N+1}} - S_{\mathrm{N}}) f(\Delta E) + S_{\mathrm{N}}} \right], \tag{19}$$

where $\Delta E = E_{\mathrm{g,N}} - E_{\mathrm{g,N+1}} + eV_{\mathrm{g}}$ is the energy difference between the benzene ground states with N and $N+1$ electrons diminished by a term linear in the gate voltage. Interference effects are contained in the overlap factor $\Lambda_{\mathrm{N,N+1}}$,

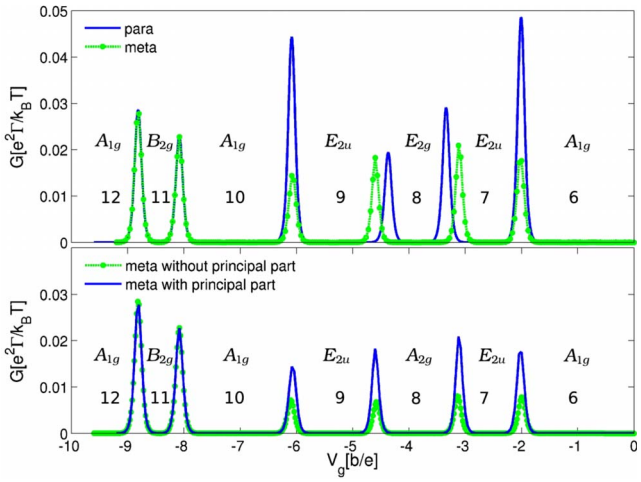

FIG. 3. (Color online) Conductance of the benzene I-SET as a function of the gate voltage. Clearly visible are the peaks corresponding to the transitions between ground states with N and $N+1$ particles. In the low conductance valleys the state of the system has a definite number of particles and symmetry as indicated in the upper panel for the para; in the lower for the metaconfiguration. Selective conductance suppression when changing from the meta to the paraconfiguration is observed.

$$\Lambda_{\mathrm{N,N+1}} = \frac{\left| \sum_{nm\tau} \langle N,n|d_{\mathrm{L}\tau}|N+1,m\rangle\langle N+1,m|d_{\mathrm{R}\tau}^{\dagger}|N,n\rangle \right|^2}{S_{\mathrm{N}} S_{\mathrm{N+1}} \sum_{nm\alpha\tau} |\langle N,n|d_{\alpha\tau}|N+1,m\rangle|^2},$$

where n and m label the S_{N}-fold and $S_{\mathrm{N+1}}$-fold degenerate ground states with N and $N+1$ particles, respectively. In order to make the interference effects more visible we remind that $d_{\mathrm{R}\tau}^{\dagger} = \mathcal{R}_{\phi}^{\dagger} d_{\mathrm{L}\tau}^{\dagger} \mathcal{R}_{\phi}$, with $\phi = \pi$ for the paraconfiguration while $\phi = 2\pi/3$ for the metaconfiguration. Due to the behavior of all eigenstates of H_{ben}^{0} under discrete rotation operators with angles multiples of $\pi/3$, we can rewrite the overlap factor as

$$\Lambda_{\mathrm{N,N+1}} = \frac{\left| \sum_{nm\tau} |\langle N,n|d_{\mathrm{L}\tau}|N+1,m\rangle|^2 e^{i\phi_{nm}} \right|^2}{S_{\mathrm{N}} S_{\mathrm{N+1}} 2 \sum_{nm\tau} |\langle N,n|d_{\mathrm{L}\tau}|N+1,m\rangle|^2}, \tag{20}$$

where ϕ_{nm} encloses the phase factors coming from the rotation of the states $|N,n\rangle$ and $|N+1,m\rangle$.

The energy nonconserving terms neglected in Eq. (19) influence only the dynamics of the coherences between orbitally degenerate states. Thus, Eq. (19) provides an exact description of transport for the paraconfiguration, where orbital degeneracy is cancelled. Even if Eq. (19) captures the essential mechanism responsible for the conductance suppression, we have derived an exact analytical formula also for the metaconfiguration, and we present it in Appendix B.

In Fig. 3 we present an overview of the results of both the para and the metaconfiguration. A direct comparison of the conductance (including energy nonconserving terms) in the two configurations is displayed in the upper panel. The lower panel illustrates the effect of the energy nonconserving terms

on the conductance in the metaconfiguration. The number of p_z electrons on the molecule and the symmetry of the lowest energy states corresponding to the conductance valleys are reported. The symmetries displayed in the upper panel belong to the (effective) ground states in the paraconfiguration; the corresponding symmetries for the metaconfiguration are shown in the lower panel.

Figure 3 shows that the results for the para and the metaconfiguration coincide for the $10 \leftrightarrow 11$ and $11 \leftrightarrow 12$ transitions. The ground states with $N=10,11,12$ particles have A- or B-type symmetries. They are therefore orbitally nondegenerate, no interference can occur, and thus the transitions are invariant under configuration change. For every other transition we see a noticeable difference between the results of the two configurations (Fig. 3). In all these transitions one of the participating states is orbitally degenerate. First we notice that the linear conductance peaks for the $7 \leftrightarrow 8$ and $8 \leftrightarrow 9$ transitions in the paraconfiguration are *shifted* with respect to the corresponding peaks in the metaconfiguration. The selection of an effective symmetric Hilbert space associated to the paraconfiguration reduces the total degeneracy by canceling the orbital degeneracy. In addition, the ground-state energy of the four- and eight-particle states is different in the two configurations since in the paraconfiguration the *effective* ground state is in reality the first excited state. The degeneracies S_N, S_{N+1} of the participating states as well as the ground-state energy are both entering the degeneracy term of Eq. (19),

$$\Delta = -\frac{f'(\Delta E)}{(S_{N+1} - S_N) f(\Delta E) + S_N}, \tag{21}$$

and determine the shift of the conductance peaks.

Yet, the most striking effect regarding transitions with orbitally degenerate states participating is the *systematic suppression* of the linear conductance when changing from the para to the metaconfiguration. The suppression is appreciable despite the conductance enhancement due to the energy nonconserving terms (see Fig. 3, lower panel). Thus, we will for simplicity discard them in the following discussion.

The conductance is determined by the combination of two effects: the reduction to the symmetric Hilbert space in the paraconfiguration and the interference effects between degenerate orbitals in the metaconfiguration. The reduction to the symmetric Hilbert space implies also a lower number of conducting channels (see Table III). One would expect a suppression of transport in the paraconfiguration. The actual opposite behavior is partially explained by Δ_{max} (see Table III) which is higher in the paraconfiguration.

The second effect determining transport is the interference between the E-type states, which is accounted for in the overlap factor Λ. The overlap factor is basis independent; thus, we can write the transition probabilities for the $6 \leftrightarrow 7$ transition as $|\langle 6_g | d_{L\tau} | 7_g \ell \tau \rangle|^2 = C$, where τ and ℓ are the spin and the quasiangular momentum quantum number, respectively. The transition probabilities have the same value since all four seven-particle states are in this basis equivalent (see Appendix C). Under the C_2 rotation the symmetric seven-particle ground state does not acquire any phase factor. Under the C_3 rotation, however, the two orbitally degenerate states acquire different phase factors, namely, $e^{i4\pi/3}$ and $e^{-i4\pi/3}$, respectively. Thus the overlap factors Λ for the $6 \leftrightarrow 7$ transition are

TABLE III. Number of channels participating to transport, overlap factor, and resonance value of the degeneracy term in the para and the metaconfiguration for the $6 \leftrightarrow 7$ transition peak. It is $C = |\langle 6_g | d_{L\tau} | 7_g \ell \tau \rangle|^2$, where τ and ℓ are the spin and the quasiangular momentum quantum numbers, respectively. The values of Δ_{max} are given for $k_B T = 0.04|b|$.

	No. of channels $S_N S_{N+1}$	Overlap factor Λ	Degeneracy term Δ_{max} $[1/k_B T]$
PARA	2	C	0,17
META	4	$\frac{1}{8}C$	0,11

$$\Lambda_{para} = \frac{1}{2 \cdot 8C} |4C|^2 = C,$$

$$\Lambda_{meta} = \frac{1}{4 \cdot 8C} |2Ce^{+i4\pi/3} + 2Ce^{-i4\pi/3}|^2 = \frac{1}{8}C.$$

The linear conductance is determined by the product among the number of conducting channels, the overlap factor, and the degeneracy term. Yet, it is the *destructive interference* between degenerate E-type orbitals, accounted for in the overlap factor Λ, that gives the major contribution to the strong suppression of the conductance in the metaconfiguration.

B. NDC and current blocking

Interference effects between orbitally degenerate states are also affecting nonlinear transport, producing in the *meta*-configuration current blocking and thus NDC at the border of the six-particle state diamond (Fig. 2). The upper panel of Fig. 4 shows the current through the benzene I-SET contacted in the metaconfiguration as a function of the bias voltage. The current is given for parameters corresponding to the white dashed line of Fig. 2. In this region only the six- and seven-particle ground states are populated.

At low bias the six-particle state is mainly occupied. As the bias is raised, transitions $6 \leftrightarrow 7$ occur and current flows. Above a certain bias threshold a blocking state is populated and the current drops. For the understanding of this nonlinear current characteristics, we have to take into account energy conservation, the Pauli exclusion principle, and the interference between participating states. For the visualization of the interference effects, we introduce the transition probability (averaged over the z coordinate and the spin σ),

$$P(x,y;n,\tau) = \lim_{L\to\infty} \sum_{\sigma} \frac{1}{2L} \int_{-L/2}^{L/2} dz |\langle 7_g n \tau | \psi_\sigma^\dagger(\mathbf{r}) | 6_g \rangle|^2, \tag{22}$$

for the *physical* seven-particle basis, i.e., the seven-particle basis that diagonalizes the stationary density matrix at a fixed

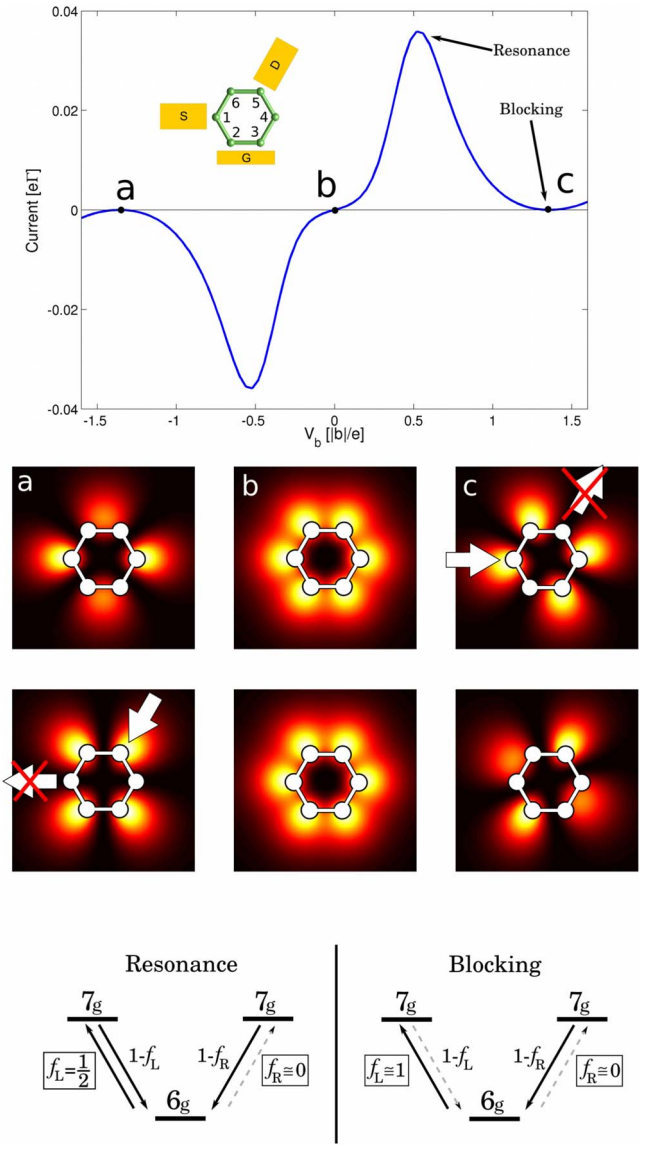

FIG. 4. (Color online) Upper panel—current through the benzene I-SET in the metaconfiguration calculated at bias and gate voltage conditions indicated by the dashed line of Fig. 2. A pronounced NDC with current blocking is visible. Middle panels—transition probabilities between the six-particle and each of the two seven-particle ground states for bias voltage values labeled *a*-*c* in the upper panel. The transition to a blocking state is visible in the upper (lower) part of the *c* (*a*) panels. Lower panels—sketch of the energetics for the $6\rightarrow 7$ transition in the metaconfiguration at bias voltages corresponding to the resonance current peak and current blocking as indicated in the upper panel of this figure.

bias. Here τ is the spin quantum number; $n=1,2$ labels the two states of the physical basis which are linear combinations of the orbitally degenerate states $|7_g \ell \tau\rangle$ and can be interpreted as conduction channels. Each of the central panels of Fig. 4 are surface plots of Eq. (22) at the different bias voltages *a*-*c*. The seven-particle ground states can interfere and thus generate nodes in the transition probability at the contact atom close to one or the other lead but, in the metaconfiguration, never at both contact atoms at the same time.

Energetic considerations are illustrated in the lower panels of Fig. 4 for two key points of the current curve at positive biases. The left panel corresponds to the resonance peak of the current. Due to energy conservation, electrons can enter the molecule only from the left lead. On the contrary the exit is allowed at both leads. The current is suppressed when transitions occur to a state which cannot be depopulated (a blocking state). Since, energetically, transmissions to the six-particle state are allowed at both leads, each seven-particle state can always be depopulated and no blocking occurs.

The current blocking scenario is depicted in the lower right panel of Fig. 4. For large positive bias the transition from a seven-particle ground state to the six-particle ground state is energetically forbidden at the left lead. Thus, for example, the *c* panel in Fig. 4 visualizes the current blocking situation yielding NDC: while for both channels there is a nonvanishing transition probability from the source lead to the molecule, for the upper channel a node prevents an electron from exiting to the drain lead. In the long time limit the blocking state gets fully populated while the nonblocking state is empty. At large negative bias the blocking scenario is depicted in panel *a* that shows the left-right symmetry obtained by a reflection through a plane perpendicular to the molecule and passing through the carbon atoms 6 and 3.

The temperature sets the scale of the large bias condition, and, correspondingly, the width of the current peak presented in Fig. 4 grows with it. The peak is not symmetric though. Its shape depends also on the energy renormalization introduced by the coupling to the leads[45] [principal part contribution in the GME Eq. (7)]. The result is a nonlinear dependence of the peak width with the temperature. We remark that only a description that retains coherences between the degenerate seven-particle ground states correctly captures NDC at both positive and negative biases.

In contrast to the $6\rightarrow 7$ transition, one does *not* observe NDC at the border of the seven-particle Coulomb diamond but rather a strong suppression of the current. The upper panel of Fig. 5 shows the current through the benzene I-SET contacted in the metaconfiguration as a function of the bias voltage corresponding to the white dotted line of Fig. 2. The middle panels show the transition probabilities between each of the seven-particle and the six-particle ground states.

The lower panel of Fig. 5 shows a sketch of the energetics at positive bias corresponding to the "expected" resonance peak. Here electrons can enter the molecular dot at both leads, while the exit is energetically forbidden at the left lead. Thus, if the system is in the seven-particle state which is blocking the right lead, this state cannot be depopulated, becoming the blocking state.

On the other hand, transitions from the six-particle ground state to both seven-particle ground states are equally probable. Thus the blocking state will surely be populated at some time. The upper plot of the *b* panel in Fig. 5 shows the transition probability to the blocking state that accepts electrons from the source lead but cannot release electrons to the drain.

We just proved that in this case the current blocking situation occurs already at the resonance bias voltage. For a higher positive bias, the transition probability from the blocking state at the drain lead increases and current can

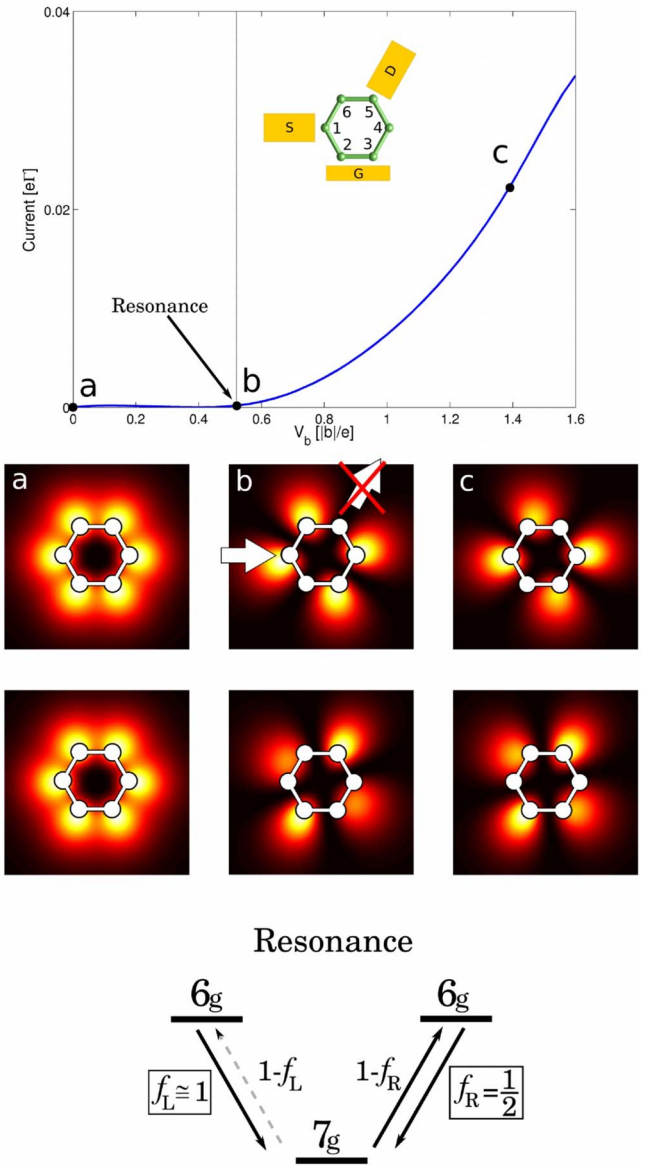

FIG. 5. (Color online) Upper panel—current through the benzene I-SET in the metaconfiguration calculated at bias and gate voltage conditions indicated by the dotted line of Fig. 2. No NDC is visible. Middle panels—transition probabilities between each of the seven-particle and the six-particle ground state for bias voltage values labeled as *a*-*c* in the upper panel. Lower panel—sketch of the energetics for the $7\rightarrow 6$ transition in the metaconfiguration at bias voltage corresponding to the expected resonance peak. (compare to Fig. 4).

flow. This effect, though, can be captured only by taking into account also the energy nonconserving terms in Eq. (7).

In the *para*configuration, the current as a function of the bias voltage is shown in Fig. 6. The current is given for parameters corresponding to the white dashed line of Fig. 2. In this case, no interference effects are visible. We see instead the typical steplike behavior of the current in the Coulomb blockade regime.

The panels on the right are the surface plots of

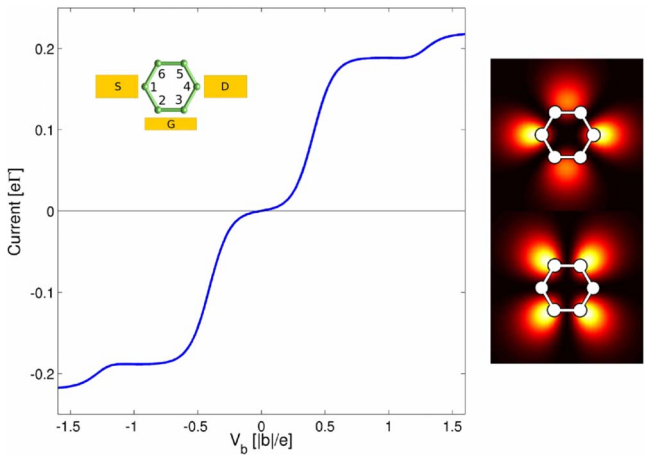

FIG. 6. (Color online) Left panel—current through the benzene I-SET in the paraconfiguration calculated at bias and gate voltage conditions indicated by the dashed line of Fig. 2. No interference effects are visible. Right panels—transition probabilities between the six-particle and the symmetric and antisymmetric seven-particle ground states.

$$P(x,y;\tau) = \lim_{L\to\infty} \sum_{\sigma} \frac{1}{2L} \int_{-L/2}^{L/2} dz |\langle 7_g \tau; (a)sym | \psi_\sigma^\dagger(\mathbf{r}) | 6_g \rangle|^2. \tag{23}$$

The upper plot shows the transition probability to the symmetric seven-particle state and the lower to the antisymmetric. Remember that in the paraconfiguration only the symmetric states contribute to transport. Evidently the symmetric state is in the paraconfiguration nonblocking. Additionally, since the coherences between orbitally degenerate states and therefore the energy nonconserving terms do not play any role in the transport, the physical basis states are not bias dependent. Thus in the paraconfiguration there are always nonblocking states populated and no NDC can occur.

IV. REDUCED SYMMETRY

In this section we study the effect of reduced symmetry on the results presented previously. We generalize the model Hamiltonian by taking into account the perturbations on the molecule due to the contacts and the bias voltage. The contact between molecule and leads is provided by different anchor groups. These linkers are coupled to the contact carbon atoms over a σ bond thus replacing the corresponding benzene hydrogen atoms. Due to the orthogonality of π and σ orbitals, the anchor groups affect in first approximation only the σ orbitals of benzene. In particular the different electron affinities of the atoms in the linkers imply a redistribution of the density of σ electrons. Assuming that transport is carried by π electrons only, we model the effect of this redistribution as a change in the on-site energy for the p_z orbitals of the contact carbon atoms,

$$H'_{\text{ben}} := H_{\text{contact}} = \xi_c \sum_{\alpha\sigma} d^\dagger_{\alpha\sigma} d_{\alpha\sigma}, \quad \alpha = L,R, \tag{24}$$

where $R=4,5$, respectively, in the para and metaconfiguration and $L=1$ in both setups.

TABLE IV. Point groups to which the molecule belongs under the influence of the contacts and the external bias potential.

	PARA	META
Contact perturb.	D_{2h}	C_{2v}
Bias perturb.	C_{2v}	C_{2v}

We also study the effect of an external bias on the benzene I-SET. In particular we release the strict condition of potential drop all concentrated at the lead-molecule interface. Nevertheless, due to the weak coupling of the molecule to the leads, we assume that only a fraction of the bias potential drops across the molecule, similar to Hettler *et al.*[28] For this residual potential we take the linear approximation $V_b(\mathbf{r}) = -\frac{V_b}{a}(\mathbf{r}\cdot\hat{\mathbf{r}}_{sd}/a_0)$, where we choose the center of the molecule as the origin and $\hat{\mathbf{r}}_{sd}$ is the unity vector directed along the source to drain direction. $a_0 = 1.43$ Å is the bond length between two carbon atoms in benzene; a is the coefficient determining the intensity of the potential drop over the molecule. Since the p_z orbitals are strongly localized, we can assume that this potential will not affect the intersite hopping but only the on-site term of the Hamiltonian,

$$H'_{ben} := H_{bias} = e\sum_{i\sigma} \xi_{b_i} d^\dagger_{i\sigma} d_{i\sigma} \tag{25}$$

with $\xi_{b_i} = \int d\mathbf{r} p_z(\mathbf{r}-\mathbf{R}_i) V_b(\mathbf{r}) p_z(\mathbf{r}-\mathbf{R}_i)$.

Under the influence of the contacts or the bias potential, the symmetry of the molecule changes. Table IV shows the point groups to which the molecule belongs in the perturbed setup. This point groups have only A- and B-type irreducible representations. Thus the corresponding molecular orbitals do not exhibit orbital degeneracy.

No interference effects influence the transport in the para-configuration. Thus we do not expect its transport characteristics to be qualitatively modified by the new setup with the corresponding loss of degeneracies.

In the metaconfiguration, on the other hand, interferences between orbitally degenerate states play a crucial role in the explanation of the occurring transport features. Naïvely one would therefore expect that neither conductance suppression nor NDC and current blocking occur in a benzene I-SET with reduced symmetry. Yet we find that, under certain conditions, the mentioned transport features are robust under the lowered symmetry.

The perturbations due to the contacts and the bias lead to an expected level splitting of the former orbitally degenerate states. Very different current-voltage characteristics are obtained depending on the relation between the energy splitting δE and other two important energy scales of the system: the tunneling rate Γ and the temperature T. In particular, when $\delta E \ll \Gamma \ll T$, interference phenomena persist. In contrast, when $\Gamma < \delta E \ll T$, interference phenomena disappear despite the fact that, due to temperature broadening, the two states still cannot be resolved. In this regime, due to the asymmetry in the tunneling rates introduced by the perturbation, standard NDC phenomena (see Fig. 8) occur.

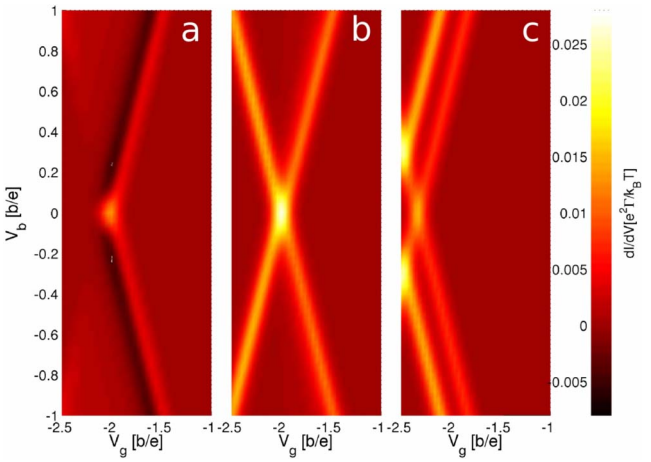

FIG. 7. (Color online) Close-up views of the stability diagram around the $6 \leftrightarrow 7$ resonance for the system under contact perturbation. The perturbation strength grows from left to right The parameter that describes the contact effect assumes the values $\xi_c = 0.15\Gamma, 2\Gamma, 15T$ from left to right, respectively, and $T = 10\Gamma$.

In the absence of perfect degeneracy, we abandon the strict secular approximation scheme that would discard the coherences in the density matrix between states with different energies. We adopt instead a softer approximation by retaining also coherences between quasidegenerate states. Since they have Bohr frequencies comparable to the tunneling rate, they influence the stationary density matrix. Formulas for the GME and the current taking into account these coherence terms are presented in Appendix A.

Figure 7 shows from left to right close-up views of the stability diagram for the setup under the influence of increasing *contact perturbation* around the $6 \leftrightarrow 7$ resonance. The orbital degeneracy of the seven-particle states is lifted, and the transport behavior for the $6 \leftrightarrow 7$ transition depends on the energy difference between the formerly degenerate seven-particle ground states. In panel a the energy difference is so small that the states are quasidegenerate: $\delta E \ll \hbar\Gamma \ll k_B T$. As expected, we recover NDC at the border of the six-particle diamond and current suppression at the border of the seven-particle diamond, such as in the unperturbed setup.

Higher on-site energy shifts correspond to a larger level spacing. Panel b displays the situation in which the latter is of the order of the level broadening but still smaller than the thermal energy ($\delta E \simeq \hbar\Gamma \ll k_B T$): no interference causing NDC and current blocking can occur. Yet, due to thermal broadening, we cannot resolve the two seven-particle states.

Eventually, panel c presents the stability diagram for the case $\delta E > k_B T > \hbar\Gamma$: the level spacing between the seven-particle ground and first excited state is now bigger than the thermal energy; thus, the two transition lines corresponding to these states are clearly visible at the border of the six-particle stability diamond.

Figure 8 shows close-up views of the stability diagram for the setup under the influence of the *bias perturbation* at the border of the six- and seven-particle diamonds. The same region is plotted for different strengths of the external potential over the molecule. In contrast to the contact perturbation, the amount of level splitting of the former degenerate states

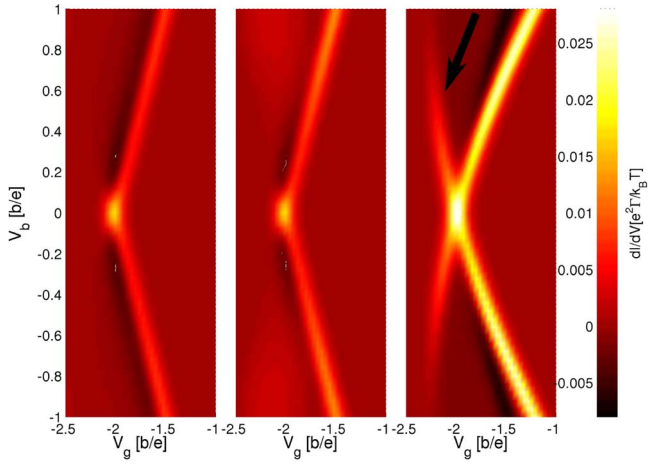

FIG. 8. (Color online) Close-up views of the stability diagram around the $6 \leftrightarrow 7$ resonance for the system under the effect of the bias potential, displayed for different strengths of the electrostatic potential drop over the molecule. The parameter that describe the strength of the electrostatic drop over the molecule assumes the values $a=25, 12, 0.6$ from left to right, respectively.

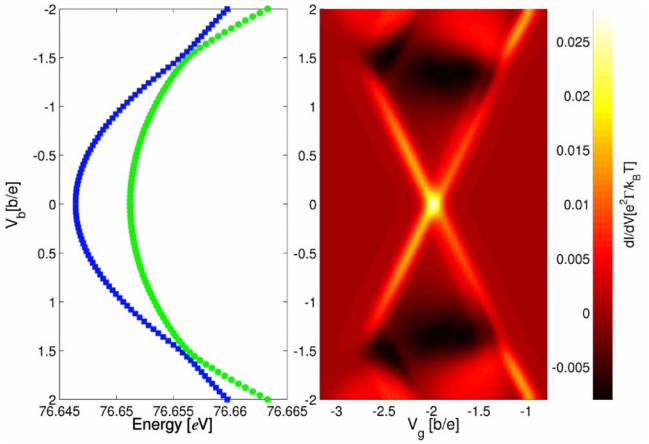

FIG. 9. (Color online) Combination of the bias and contact perturbations. Left panel—energy levels of the seven-particle ground and first excited state as functions of the bias voltage. Right panel—stability diagram around the $6 \leftrightarrow 7$ resonance. The perturbation parameters are in this case $\xi_c = 2\Gamma$ and $a=12$.

is here bias dependent. This fact imposes a bias window of interference visibility. The bias must be small enough for the seven-particle states to be quasidegenerate and at the same time bigger than the thermal energy so that the occurring NDC is not obscured by the thermally broadened conductance peak. A strong electrostatic potential perturbation closes the bias window and no interference effect can be detected.

Panel *a* of Fig. 8 represents the weak perturbation regime with no qualitative differences with the unperturbed case. The typical fingerprints of interference (NDC at the border of the six-particle diamond and current blocking for the $7 \rightarrow 6$ transition) are still visible for intermediate perturbation strength (panel *b*) but this time only in a limited bias window. Due to the perturbation strength, at some point in the bias, the level splitting is so big that the quasidegeneracy is lifted and the interference effects are destroyed. In panel *c* the quasidegeneracy is lifted in the entire bias range. There is NDC at the border of the six-particle diamond, but it is not accompanied by current blocking as proven by the excitation line at the border of the seven-particle diamond (see arrow): no interference occurs. The NDC is here associated to the sudden opening of a slow current channel, the one involving the six-particle ground state and the seven-particle (nondegenerate) excited state (standard NDC).

Figure 9 refers to the setup under both the *bias and contact perturbations*. The left panel shows the energy of the lowest seven-particle states as a function of the bias. In the right panel we present the stability diagram around the $6 \leftrightarrow 7$ resonance. NDC and current blocking are clearly visible only in the bias region where, due to the combination of bias and contact perturbation, the quasidegeneracy of the two seven-particle states is reestablished. Also the fine structure in the NDC region is understandable in terms of interference if in the condition of quasidegeneracy we take into account the renormalization of the level splitting due to the energy nonconserving terms.

Interference effects predicted for the unperturbed benzene I-SET are robust against various sources of symmetry breaking. Quasidegeneracy, $\delta E \ll \hbar\Gamma \ll k_B T$, is the necessary condition required for the detection of the interference in the stability diagram of the benzene I-SET.

V. CONCLUSIONS

In this paper we analyze the transport characteristics of a benzene I-SET. Two different setups are considered, the para and the metaconfiguration, depending on the position of the leads with respect to the molecule.

Within an effective p_z orbital model, we diagonalize exactly the Hamiltonian for the molecule. We further apply a group-theoretical method to classify the many-body molecular eigenstates according to their symmetry and quasiangular momentum. With the help of this knowledge we detect the orbital degeneracy and, in the paraconfiguration, we select the states relevant for transport.

We introduce a generic interference condition [Eq. (1)] for I-SETs in terms of the tunneling transitions *amplitudes* of degenerate states with respect to the source and drain leads. By applying it to the benzene I-SET we predict the existence of interference effects in the metaconfiguration In order to study the dynamics of the molecular I-SET, we use a density matrix approach which starts from the Liouville equation for the total density operator and which enables the treatment of quasidegenerate states.

The stability diagrams for the two configurations show striking differences. In the linear regime a selective conductance suppression is visible when changing from the para to the metaconfiguration. Only transitions between ground states with well-defined particle number are affected by the change in the lead configuration. With the help of the group-theoretical classification of the states we recognize in this effect a fingerprint of the *destructive interference* between orbitally degenerate states. We derive an analytical formula for the conductance that reproduces exactly the numerical

result and supports their interpretation in terms of interference. Other interference effects are also visible in the nonlinear regime where they give rise to NDC and current blocking at the border of the six-particle Coulomb diamond as well as to current suppression for transitions between seven- and six-particle states.

We provide a detailed discussion of the impact of the reduced symmetry due to linking groups between the molecule and the leads or to an electrostatic potential drop over the molecule. We classify different transport regimes and set up the limits within which the discussed transport features are robust against perturbations. We identify in the *quasidegeneracy* of the molecular states the necessary condition for interference effects.

ACKNOWLEDGMENT

We acknowledge financial support by the Deutsche Forschungsgemeinschaft within the research programs Schwerpunktprogramm 1243 and Sonderforschungsbereich 689.

APPENDIX A: GME AND CURRENT IN THE NONSECULAR APPROXIMATION

The bias and the contact perturbations in our model for a benzene I-SET lower the symmetry of the active part of the junction and consequently lift the degeneracy that appeared so crucial for the interference effects. The robustness of the latter relies on the fact that the necessary condition is rather quasidegeneracy, expressed by the relation $\delta E \ll \hbar\Gamma$.

Nevertheless, if the perfect degeneracy is violated, the secular approximation applied to obtain Eq. (7) does not capture this softer condition. We report here the general expression for the generalized master equation and the associated current operator in the Born-Markov approximation and under the only further condition (exact in absence of superconductors) that coherences between states with different particle number are decoupled from the populations and vanish exactly in the stationary limit,

$$\begin{aligned}
\dot{\sigma}^{\mathrm{N}}_{\mathrm{EE}'} = & -\frac{i}{\hbar}(E-E')\sigma^{\mathrm{N}}_{\mathrm{EE}'} - \sum_{\alpha\tau\mathrm{F}} \frac{\Gamma_\alpha}{2} \mathcal{P}_{\mathrm{NE}} \Bigg\{ d^\dagger_{\alpha\tau}\Bigg[-\frac{i}{\pi} p_\alpha (F - H^0_{\mathrm{ben}}) + f^-_\alpha (F - H^0_{\mathrm{ben}}) \Bigg] d_{\alpha\tau} \\
& + d_{\alpha\tau}\Bigg[-\frac{i}{\pi} p_\alpha (H^0_{\mathrm{ben}} - F) + f^+_\alpha (H^0_{\mathrm{ben}} - F) \Bigg] d^\dagger_{\alpha\tau} \Bigg\} \sigma^{\mathrm{N}}_{\mathrm{FE}'} \\
& - \sum_{\alpha\tau\mathrm{F}} \frac{\Gamma_\alpha}{2} \sigma^{\mathrm{N}}_{\mathrm{EF}} \Bigg\{ d^\dagger_{\alpha\tau}\Bigg[+\frac{i}{\pi} p_\alpha (F - H^0_{\mathrm{ben}}) + f^-_\alpha (F - H^0_{\mathrm{ben}}) \Bigg] d_{\alpha\tau} \\
& + d_{\alpha\tau}\Bigg[+\frac{i}{\pi} p_\alpha (H^0_{\mathrm{ben}} - F) + f^+_\alpha (H^0_{\mathrm{ben}} - F) \Bigg] d^\dagger_{\alpha\tau} \Bigg\} \mathcal{P}_{\mathrm{NE}'} \\
& + \sum_{\alpha\tau\mathrm{FF}'} \frac{\Gamma_\alpha}{2} \mathcal{P}_{\mathrm{NE}} \Bigg\{ d^\dagger_{\alpha\tau} \sigma^{\mathrm{N-1}}_{\mathrm{FF}'} d_{\alpha\tau}\Bigg[+\frac{i}{\pi} p_\alpha (E' - F') + f^+_\alpha (E' - F') - \frac{i}{\pi} p_\alpha (E - F) + f^+_\alpha (E - F) \Bigg] \\
& + d_{\alpha\tau} \sigma^{\mathrm{N+1}}_{\mathrm{FF}'} d^\dagger_{\alpha\tau}\Bigg[+\frac{i}{\pi} p_\alpha (F' - E') + f^-_\alpha (F' - E') - \frac{i}{\pi} p_\alpha (F - E) + f^-_\alpha (F - E) \Bigg] \Bigg\} \mathcal{P}_{\mathrm{NE}'}, \qquad \text{(A1)}
\end{aligned}$$

where $\sigma^{\mathrm{N}}_{\mathrm{EE}'}$ is, different from Eq. (7), in the Schrödinger picture. Equation (7) represents a special case of Eq. (A1) in which all energy spacings between states with the same particle number are either zero or much larger than the level broadening $\hbar\Gamma$. The problem of a master equation in the presence of quasidegenerate states in order to study transport through molecules has been recently addressed in the work of Schultz and von Oppen.[38] The authors claimed in their work that the singular coupling limit should be used in order to derive an equation for the density matrix in the presence of quasidegenerate states. Equation (A1) is derived in the weak coupling limit and bridges all the regimes as illustrated by Figs. 7–9.

The current operators associated to the master equation just presented read as:

$$\begin{aligned}
I_\alpha = & \frac{\Gamma_\alpha}{2} \sum_{\mathrm{NEF}\tau} \mathcal{P}_{\mathrm{NE}} \Bigg\{ d^\dagger_{\alpha\tau}\Bigg[+\frac{i}{\pi} p_\alpha (E - H^0_{\mathrm{ben}}) + f^-_\alpha (E - H^0_{\mathrm{ben}}) \Bigg] d_{\alpha\tau} \\
& + d^\dagger_{\alpha\tau}\Bigg[-\frac{i}{\pi} p_\alpha (F - H^0_{\mathrm{ben}}) + f^-_\alpha (F - H^0_{\mathrm{ben}}) \Bigg] d_{\alpha\tau} \\
& - d_{\alpha\tau}\Bigg[+\frac{i}{\pi} p_\alpha (H^0_{\mathrm{ben}} - E) + f^+_\alpha (H^0_{\mathrm{ben}} - E) \Bigg] d^\dagger_{\alpha\tau} \\
& - d_{\alpha\tau}\Bigg[-\frac{i}{\pi} p_\alpha (H^0_{\mathrm{ben}} - F) + f^+_\alpha (H^0_{\mathrm{ben}} - F) \Bigg] d^\dagger_{\alpha\tau} \Bigg\} \mathcal{P}_{\mathrm{NF}}, \qquad \text{(A2)}
\end{aligned}$$

where $\alpha = L, R$ indicates the left or right contact. Nevertheless, within the limits of derivation of the master equation,

this formula can be simplified. Actually, if $E-F \leq \hbar\Gamma$, then F can be safely substituted with E in the argument of the principal values and of the Fermi functions, with an error of order $\frac{E-F}{k_B T} < \frac{\hbar\Gamma}{k_B T}$ which is negligible (the generalized master equation that we are considering is valid for $\hbar\Gamma \ll k_B T$). The approximation $E \sim F$ breaks down only if $E-F \sim k_B T$, but this implies that $E-F \gg \hbar\Gamma$ which is the regime of validity of the secular approximation. Consequently, in this regime, terms with $E \neq F$ do not contribute to the average current because they vanish in the stationary density matrix. Ultimately we can thus reduce the current operators to the simpler form,

$$I_\alpha = \Gamma_\alpha \sum_{\mathrm{NE}\tau} \mathcal{P}_{\mathrm{NE}} \{ + d^\dagger_{\alpha\tau} [f^-_\alpha (E - H^0_{\mathrm{ben}})] d_{\alpha\tau},$$

$$- d_{\alpha\tau} [f^+_\alpha (H^0_{\mathrm{ben}} - E)] d^\dagger_{\alpha\tau}, \qquad \text{(A3)}$$

which is almost equal to the current operator corresponding to the secular approximation. The only difference is here the absence of the second projector operator that allows contributions to the current coming from coherences between different energy eigenstates.

APPENDIX B: ANALYTICAL FORMULA FOR THE LINEAR CONDUCTANCE INCLUDING THE ENERGY NONCONSERVING TERMS

In the derivation of the conductance formula (20) we neglected the energy nonconserving terms in Eq. (7). Since in the GME they appear only in the dynamics of the coherences between orbitally degenerate states, Eq. (20) is exact for the paraconfiguration, where the orbital degeneracy is cancelled. This is not the case in the metaconfiguration where the orbital (quasi-)degeneracy is essential for the description of interference. Thus we derived a generic analytical formula for the conductance, taking into account the energy nonconserving terms. It reads as

$$G_{\mathrm{N,N+1}}(\Delta E) = e^2 \Gamma \Lambda_{\mathrm{N,N+1}} \left[- \frac{S_{\mathrm{N}} S_{\mathrm{N+1}} f'(\Delta E)}{(S_{\mathrm{N+1}} - S_{\mathrm{N}}) f(\Delta E) + S_{\mathrm{N}}} \right] \left\{ 1 + \frac{\mathrm{aux}(S_{\mathrm{N}}, S_{\mathrm{N+1}}) 3\mathcal{P}^2}{16 \Lambda^2_{\mathrm{N,N+1}} (S_{\mathrm{N}} S_{\mathrm{N+1}})^2 [f^{\pm}(\Delta E)]^2 + \mathcal{P}^2} \right\}. \qquad \text{(B1)}$$

Here, it is $\Gamma = \Gamma_{\mathrm{L}} = \Gamma_{\mathrm{R}}$. $\Lambda_{\mathrm{N,N+1}}$ is the overlap factor introduced in Sec. III A, Eq. (21). The auxiliary function $\mathrm{aux}(S_{\mathrm{N}}, S_{\mathrm{N+1}})$ in the correction term is zero if there are *no* orbitally degenerate ground states involved in the transition. If one of the participating states is orbitally degenerate it is $\mathrm{aux}(S_{\mathrm{N}}, S_{\mathrm{N+1}}) = 1$. The sign in $f^{\pm}(\Delta E)$ is defined as follows: $f^+(\Delta E)$ has to be used if the N-particle ground state is orbitally degenerate. If instead the $N+1$-particle ground state exhibits orbital degeneracy, $f^-(\Delta E)$ has to be inserted. The energy nonconserving terms are included in the factor $\mathcal{P} = \mathcal{P}_{\mathrm{L}}|_{V_{\mathrm{bias}}=0} = \mathcal{P}_{\mathrm{R}}|_{V_{\mathrm{bias}}=0}$. It is defined only if a degenerate state is participating transport. In case that, e.g., the N-particle ground state is orbitally degenerate, $\mathcal{P}_\alpha$ with $\alpha = L, R$ read as

$$\mathcal{P}_\alpha = \sum_{\mathrm{E}',l} \sum_{nm} \left[\frac{i}{\pi} p_\alpha (E_{\mathrm{g,N}} - E') \right] \langle N-1, E' l | d_{\alpha\tau} | N_{\mathrm{g}}, n \rangle \langle N_{\mathrm{g}}, m | d^\dagger_{\alpha\tau} | N-1, E' l \rangle$$

$$+ \sum_{\mathrm{E}',l} \sum_{nm} \left[\frac{i}{\pi} p_\alpha (E' - E_{\mathrm{g,N}}) \right] \langle N+1, E' l | d^\dagger_{\alpha\tau} | N_{\mathrm{g}}, n \rangle \langle N_{\mathrm{g}}, m | d_{\alpha\tau} | N+1, E' l \rangle, \qquad \text{(B2)}$$

where $p_\alpha(x) = -\mathrm{Re}\, \psi[\frac{1}{2} + \frac{i\beta}{2\pi}(x - \mu_\alpha)]$ and ψ is the digamma function, as defined in Sec. II B.

APPENDIX C: TRANSITION PROBABILITIES FOR THE 6↔7 TRANSITION

In the calculation of the overlap factor Λ in Sec. III A we used the relation

$$|\langle 6_{\mathrm{g}} | d_{\mathrm{L}} | 7_{\mathrm{g}}, \ell = 2 \rangle|^2 = |\langle 6_{\mathrm{g}} | d_{\mathrm{L}} | 7_{\mathrm{g}}, \ell = -2 \rangle|^2 \qquad \text{(C1)}$$

for the transition probabilities between the six-particle ground state and the seven-particle ground states $|7_{\mathrm{g}}, \ell\rangle$, where ℓ is the eigenvalue of the quasiangular momentum. This relation is now to be proven.

Again, we take advantage of the symmetry properties of the molecular states with respect to the σ_{v} operation and to the rotation operator R_ϕ for rotations about a discrete angle $\phi = \frac{n\pi}{3}$, as introduced in Sec. II C. The starting point is the

generic relation between these two operators,

$$\mathcal{R}_\phi \sigma_v = \sigma_v \mathcal{R}_{-\phi}. \quad \text{(C2)}$$

We can now apply both sides of this relation to the seven-particle ground states $|7_g, \ell = \pm 2\rangle$,

$$\mathcal{R}_\phi \sigma_v |7_g, \ell = \pm 2\rangle = \sigma_v \mathcal{R}_{-\phi} |7_g, \ell = \pm 2\rangle. \quad \text{(C3)}$$

The seven-particle ground states $|7_g, \ell = \pm 2\rangle$ are eigenstates of each $\mathcal{R}_\phi$, and the corresponding eigenvalues are phase factors,

$$\mathcal{R}_\phi |7_g, \ell = \pm 2\rangle = e^{\mp 2i\phi} |7_g, \ell = \pm 2\rangle. \quad \text{(C4)}$$

Thus, Eq. (C3) becomes

$$\mathcal{R}_\phi (\sigma_v |7_g, \ell = \pm 2\rangle) = e^{\pm 2i\phi} (\sigma_v |7_g, \ell = \pm 2\rangle). \quad \text{(C5)}$$

Yet, according to Eq. (C4), this equation can only be valid if

$$\sigma_v |7_g, \ell = \pm 2\rangle = \lambda |7_g, \ell = \mp 2\rangle \quad \text{(C6)}$$

and, since $\sigma_v^2 = 1$, λ can only be a phase factor. For the calculation of the transition probabilities we use further the property $\sigma_v^\dagger \sigma_v = 1$. Since the left contact atom (atom 1) lies in the reflection plane σ_v, it is $\sigma_v d_L \sigma_v^\dagger = d_L$. Also, since the symmetry of the six-particle ground state is A_{1g}, it is $\sigma_v |6_g\rangle = |6_g\rangle$. Under these considerations, we can write for the transition probability to the state $|7_g, \ell = 2\rangle$

$$\begin{aligned} |\langle 6_g | d_L | 7_g, \ell = 2\rangle|^2 &= |\langle 6_g | \sigma_v^\dagger \sigma_v d_L \sigma_v^\dagger \sigma_v | 7_g, \ell = 2\rangle|^2 \\ &= |\langle 6_g | d_L \sigma_v | 7_g, \ell = 2\rangle|^2 \\ &= |\langle 6_g | d_L | 7_g, \ell = -2\rangle|^2. \end{aligned} \quad \text{(C7)}$$

[1] *Introducing Molecular Electronics*, edited by G. Cuniberti, G. Fagas, and K. Richter (Springer, Berlin, 2005).
[2] J. Park, A. N. Pasupathy, J. I. Goldsmith, C. Chang, Yu. Yaish, J. R. Petta, M. Rinkoski, J. P. Sethna, H. D. Abruna, P. L. McEuen, and D. C. Ralph, Nature (London) **417**, 722 (2002).
[3] W. Liang, M. P. Shores, M. Bockrath, J. R. Long, and H. Park, Nature (London) **417**, 725 (2002).
[4] S. Kubatkin, A. Danilov, M. Hjort, J. Cornil, J.-L. Brédas, N. Stuhr-Hansen, P. Hedegård, and T. Bjørnholm, Nature (London) **425**, 698 (2003).
[5] L. H. Yu, Z. K. Keane, J. W. Ciszek, L. Cheng, J. M. Tour, T. Baruah, M. R. Pederson, and D. Natelson, Phys. Rev. Lett. **95**, 256803 (2005).
[6] A. V. Danilov, S. Kubatkin, S. Kafanov, P. Hedegård, N. Stuhr-Hansen, K. Moth-Poulsen, and T. Bjørnholm, Nano Lett. **8**, 1 (2008).
[7] D.-H. Chae, J. F. Berry, S. Jung, F. A. Cotton, C. A. Murillo, and Z. Yao, Nano Lett. **6**, 165 (2006).
[8] M. Poot, E. Osorio, K. O'Neill, J. M. Thijssen, D. Vanmaekelbergh, C. A. van Walree, L. W. Jenneskens, and H. S. J. van der Zant, Nano Lett. **6**, 1031 (2006).
[9] H. B. Heersche, Z. de Groot, J. A. Folk, H. S. J. van der Zant, C. Romeike, M. R. Wegewijs, L. Zobbi, D. Barreca, E. Tondello, and A. Cornia, Phys. Rev. Lett. **96**, 206801 (2006).
[10] E. A. Osorio, K. O'Neill, N. Stuhr-Hansen, O. F. Nielsen, T. Bjørnholm, and H. S. J. van der Zant, Adv. Mater. **19**, 281 (2007).
[11] E. Lörtscher, H. B. Weber, and H. Riel, Phys. Rev. Lett. **98**, 176807 (2007).
[12] R. H. M. Smit, Y. Noat, C. Untiedt, N. D. Lang, M. C. van Hemert, and J. M. van Ruitenbeek, Nature (London) **419**, 906 (2002).
[13] M. Kiguchi, O. Tal, S. Wohlthat, F. Pauly, M. Krieger, D. Djukic, J. C. Cuevas, and J. M. van Ruitenbeek, Phys. Rev. Lett. **101**, 046801 (2008).
[14] A. R. Champagne, A. N. Pasupathy, and D. C. Ralph, Nano Lett. **5**, 305 (2005).
[15] L. Venkataraman, J. E. Klare, C. Nuckolls, M. S. Hybertsen, and M. L. Steigerwald, Nature (London) **442**, 904 (2006).
[16] J. Repp, G. Meyer, S. M. Stojkovic, A. Gourdon, and C. Joachim, Phys. Rev. Lett. **94**, 026803 (2005).
[17] X. Xiao, B. Xu, and N. J. Tao, Nano Lett. **4**, 267 (2004).
[18] D. I. Gittins, D. Bethell, D. J. Schiffrin, and R. J. Nichols, Nature (London) **408**, 67 (2000).
[19] M. Mayor, H. B. Weber, J. Reichert, M. Elbing, C. von Hänisch, D. Beckmann, and M. Fischer, Angew. Chem., Int. Ed. **42**, 5834 (2003).
[20] F. Chen, X. Li, J. Hihath, Z. Huang, and N. J. Tao, J. Am. Chem. Soc. **128**, 15874 (2006).
[21] L. Venkataraman, J. E. Klare, I. W. Tam, C. Nuckolls, M. S. Hybertsen, and M. L. Steigerwald, Nano Lett. **6**, 458 (2006).
[22] N. Roch, S. Florens, V. Bouchiat, W. Wernsdorfer, and F. Balestro, Nature (London) **453**, 633 (2008).
[23] D. V. Cardamone, C. A. Stafford, and S. Mazumdar, Nano Lett. **6**, 2422 (2006).
[24] A. Gagliardi, G. C. Solomon, A. Pecchia, T. Frauenheim, A. Di Carlo, N. S. Hush, and J. R. Reimers, Phys. Rev. B **75**, 174306 (2007).
[25] S.-H. Ke, W. Yang, and U. Baranger, Nano Lett. **8**, 3257 (2008).
[26] Z. Qian, R. Li, X. Zhao, S. Hou, and S. Sanvito, Phys. Rev. B **78**, 113301 (2008).
[27] H. Bruus and K. Flensberg, *Many-Body Quantum Theory in Condensed Matter Physics* (Oxford University Press, Oxford, 2004).
[28] M. H. Hettler, W. Wenzel, M. R. Wegewijs, and H. Schoeller, Phys. Rev. Lett. **90**, 076805 (2003).
[29] S. A. Gurvitz and Ya. S. Prager, Phys. Rev. B **53**, 15932 (1996).
[30] M. Braun, J. König, and J. Martinek, Phys. Rev. B **70**, 195345 (2004).
[31] B. Wunsch, M. Braun, J. König, and D. Pfannkuche, Phys. Rev. B **72**, 205319 (2005).
[32] A. Donarini, M. Grifoni, and K. Richter, Phys. Rev. Lett. **97**, 166801 (2006).
[33] U. Harbola, M. Esposito, and S. Mukamel, Phys. Rev. B **74**, 235309 (2006).
[34] L. Mayrhofer and M. Grifoni, Eur. Phys. J. B **56**, 107 (2007).
[35] S. Koller, L. Mayrhofer, and M. Grifoni, New J. Phys. **9**, 348 (2007).

[36] J. N. Pedersen, B. Lassen, A. Wacker, and M. H. Hettler, Phys. Rev. B **75**, 235314 (2007).
[37] G. Begemann, D. Darau, A. Donarini, and M. Grifoni, Phys. Rev. B **77**, 201406(R) (2008); **78**, 089901(E) (2008).
[38] M. G. Schultz and F. von Oppen, arXiv:0812.1491 (unpublished).
[39] J. Linderberg and Y. Öhrn, J. Chem. Phys. **49**, 716 (1968).
[40] R. Pariser and R. G. Parr, J. Chem. Phys. **21**, 466 (1953).
[41] J. A. Pople, Trans. Faraday Soc. **49**, 1375 (1953).
[42] W. Barford, *Electronic and Optical Properties of Conjugated Polymers* (Clarendon Press, Oxford, 2005).
[43] K. Kaasbjerg and K. Flensberg, Nano Lett. **8**, 3809 (2008).
[44] K. Blum, *Density Matrix Theory and Applications* (Plenum Press, New York, 1996).
[45] A. Donarini, G. Begemann, and M. Grifoni, arXiv:0904.0167 (unpublished).